Optical projection tomography of fluorescent microscopic specimens using lateral translation of tube lens

YONGJIN SUNG[1,*]

[1]College of Engineering & Applied Science, University of Wisconsin, Milwaukee, WI 53211, USA
[*]ysung4@uwm.edu

Compiled April 11, 2023

Optical projection tomography is a three-dimensional (3D) fluorescence imaging technique, which acquires the projection images for varying orientations of the sample using a large depth of field. OPT is typically applied to a millimeter-sized specimen, because the rotation of a microscopic specimen is challenging and not compatible with live cell imaging. In this letter, we demonstrate fluorescence optical tomography of a microscopic specimen by laterally translating the tube lens of a wide-field optical microscope, which allows for high-resolution OPT without rotating the sample. The cost is the reduction of the field of view to about 1/2 along the direction of the tube lens translation. Using bovine pulmonary artery endothelial cells and 0.1 μm beads, we compare the 3D imaging performance of the proposed method with that of the conventional objective-focus scan method.

http://dx.doi.org/10.1364/ao.XX.XXXXXX

Optical projection tomography (OPT) records the 3D distribution of fluorophores in a specimen by recording a series of images while rotating the imaged specimen[1]. For each orientation of the specimen, a large depth of field (DOF) ensures that the recorded image is a projection of the 3D fluorophore distribution. From the projection images recorded for varying orientations of the sample, the 3D fluorophore distribution can be reconstructed as in X-ray computed tomography[2]. OPT has found many important applications by allowing for 3D fluorescence imaging of a millimeter-sized specimen, filling the gap between conventional optical microscopy and magnetic resonance imaging[3]. There is a trade-off between the resolution and the DOF, i.e., the maximum thickness of the specimen that can be imaged[4]. Typically, the resolution is inversely proportional to the numerical aperture (NA) of the objective lens whereas the DOF is inversely proportional to the square of the NA[5]. For example, to double the DOF, one has to worsen the resolution by a factor of four. This is why Sharpe, in his 2002 paper[1], describes a trick where they only have half the specimen in the DOF (the front half) as this allows to retrieve a factor of square root of two in resolution at the expense of having to scan over 360°(as opposed to 180° in conventional X-ray computed tomography). Using a small DOF, OPT has also been demonstrated for high-resolution imaging of single cells[6]. A challenge with single-cell imaging using OPT is the requirement for rotating the microscopic specimen. For the rotation, the cells are typically fixed and embedded in optical gel within a tube, which is rotated using a motorized stage[6]. Alternatively, the cells can be optically trapped and rotated using a shear flow in a microfluidic channel[7]. Although these sample rotation methods can provide nearly isotropic resolution, they are not suitable for imaging the adherent cells growing on the surface of a dish or the cryo-sectioned tissues. In recent studies on snapshot optical tomography using a micro-lens array as a tube lens[8, 9], we have shown that the viewing angles of the lenslets change with their lateral distances from the optical axis. With snapshot optical tomography, we can record all the projection images simultaneously; however, each lenslet in the micro-lens array spans only a small aperture, which limits the angle of acceptance, and thus the resolution. The angular sampling is also sparse, and the angular sampling rate can be increased only at the cost of reduced aperture size (i.e., reduced transverse resolution). In this study, we demonstrate high-resolution OPT by laterally translating the tube lens of a conventional wide-field fluorescence microscope. In comparison with snapshot optical tomography, the method demonstrated here (called sliding tomography) uses the full aperture of the objective lens, and the resolution of each projection image is not limited by the aperture of the tube lens. The angular sampling rate can also be increased without lowering the transverse resolution. The proposed method can be applied to any specimens that can be imaged with a conventional microscope, providing the improvement of the axial resolution by 23% in comparison with the objective-focus scan method for the same numerical aperture (NA).

Figure 1 shows a schematic diagram of the imaging geometry used in this study. For the light source, we combined three individually-controlled light-emitting diodes (Thorlabs, M385L2, M505L4, and M565L3) using two dichroic beam splitters (Thorlabs, DMLP425R and DMLP550R). The excitation light was delivered to the sample through the fluorescence filter cube (FFC) equipped with a triple-band filter set (Semrock, DA/FI/TX-3X). The emitted light was collected by the x100 objective lens (Olympus, UPLFLN100XOI2-2) with the aperture adjusted to the smallest size, producing the minimum NA of 0.6. The objective lens

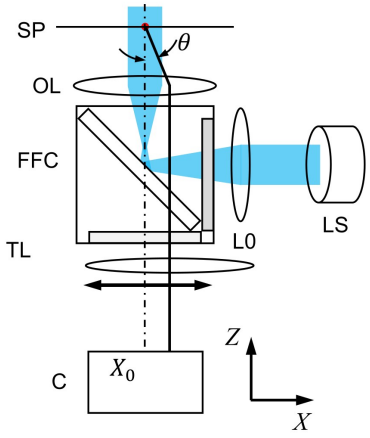

Fig. 1. Schematic diagram of the imaging geometry used in this study. SP: sample plane; OL: objective lens; TL: tube lens; LS: light source; L0: lens; FFC: fluorescence filter cube; and C: camera. The dash-dot line represents the optical axis (Z) of the objective lens, and the tube lens is translated along the X direction.

(OL) was mounted on a piezo stage (Edmund Optics, 85-008) for the objective-focus scan, which was used for comparison with the proposed method. The tube lens (TL) with the focal length of 100 mm was mounted on a motorized translation stage (Zaber, VSR20A-T3A-MC10T3) for lateral translation. The camera (C) was placed at the back focal plane of TL, where the image is formed. To record the images, we used an electron-multiplying charge-coupled device (EMCCD) camera (Andor, iXon Ultra 888) with the pixel size of 13 µm. The magnification was 55.6 and the pixel resolution was 0.23 µm. For synchronous control of the translation stages and the EMCCD camera, we used a lab-built control program written in LabVIEW (National Instruments).

For a lateral translation of the tube lens by X_0, the recorded image is a projection of the 3D fluorescence distribution along the viewing angle ϑ given by Eq. (1)[8].

$$\vartheta = \sin^{-1}\left[(1/n_0)\tan^{-1}\left[X_0/(F_{OL}^2 - X_0^2)^{1/2}\right]\right], \quad \textbf{(1)}$$

where n_0 is the refractive index of the medium in which the sample is immersed, and F_{OL} is the focal length of the objective lens. Alternatively, the viewing angle can be calculated with Eq. (2). For the derivation of Eq. (2), we assume the image formed by a conventional microscope is relayed by two lenses of the same focal length as the tube lens. When the second relay lens is laterally translated by X_0, the viewing angle at the image plane is given by $\tan^{-1}(X_0/F_{TL})$. Using the Abbe sine condition, the viewing angle at the sample plane is given by Eq. (2). Eq. (2) produces a slightly different result from the angle calculated with Eq. (1) for a large amount of lateral translation; however, its impact on the reconstructed image is not noticeable.

$$\vartheta = \sin^{-1}\left[(M/n_0)\tan^{-1}(X_0/F_{TL})\right], \quad \textbf{(2)}$$

where M is the magnification factor (55.6), and F_{TL} is the focal length of the tube lens (100 mm).

To demonstrate the proposed technique, we imaged bovine pulmonary artery endothelial (BPAE) cells (Thermo Fisher, F36924) with the mitochondria, F-actins, and nuclei stained with MitoTracker Red CMXRos, Alexa Fluor 488 Phalloidin, and DAPI, respectively. To measure the 3D point spread function (PSF), we prepared 0.1 µm fluorescent beads (Thermo Fisher, F13839) mounted in FluorSave medium (Millipore, 345789). Three drops of the bead solution was put on a microscope slide and dried by air. A drop of FluorSave was added to the slide and a coverslip was put on the top. The sample slide was used after 3 hours. Translating the tube lens changes the position of the image on the camera. To obtain the relationship between the tube lens translation and the image position on the camera, we acquired a series of images of a 1 µm fluorescent bead (Thermo Fisher, F13839) while translating the tube lens. The sample slide was prepared similarly to the 0.1 µm beads in FluorSave medium with the refractive index of 1.358. For the objective lens, the immersion oil (Thorlabs, MOIL-30) of refractive index 1.518 was used.

The imaging procedure is as follows. First, the sample to be imaged was moved to the center of the field of view. For imaging fluorescent beads, the objective focus was placed at the center of the beads, where the boundaries were seen most clearly. For the BPAE cells, the objective focus was adjusted to show all the labeled organelles (mitochondria, F-actins, and nuclei) at about the same visibility. The images were recorded with the maximum EM gain of 300 and the exposure time of 200 msec. The power of the LEDs were adjusted to achieve the maximum fluorescence intensity at about 70% of the pixel saturation level. A total of 110 images were acquired while laterally translating the tube lens with the step size of 20 µm. The lateral translation of ±1.1 mm corresponds to an angular scan within a ±26.7° range. The total data acquisition time was about 20 seconds. The data acquisition speed was limited by the weak fluorescence signal, and thus the long exposure time. Using 1 µm beads, we recorded the amount of lateral shift of each image as the tube lens is translated. In each recorded image, the bead region was identified using thresholding and the coordinates of the centroid were determined. The centroid locations were used to coregister all the projection images. The data acquired with the 1 µm bead was used to process all the other dataset. The acquired projection images were used to synthesize a 3D tomogram using the Fourier slice theorem[2], which maps the Fourier transform of each projection image onto a slice of the object's spectrum in the 3D spatial frequency space. Noteworthy, the Fourier slice theorem was originally derived for a detector that rotates with the source and remains perpendicular to the viewing direction. The imaging geometry used in this study corresponds to the case of rotating only the source while the detector is fixed and remains perpendicular to the optical axis, Z, throughout the measurements. In this case, the Fourier transform of each projection image is mapped onto the tilted plane in the 3D spatial frequency space along the K_Z direction, instead of the viewing direction, as shown in Fig. 2. For more detailed description of the reconstruction, the readers are referred to our recent work[8].

Figures 3(a) and 3(b) show two horizontal cross sections of the 3D tomogram obtained with sliding tomography. The two images are axially separated by 3.3 µm. Figures 3(d) and 3(e) are wide-field images obtained with the objective-focus scan for the same field of view and at the heights corresponding to Figs. 3(a) and 3(b), respectively. A small region in Fig. 3(a) is magnified and shown in Fig 3(c), together with the intensity profile across two actin filaments. The same region in Fig. 3(d) is magnified and shown in Fig 3(f), together with the intensity profile across the two actin filaments. Figure 3(a) shows the actin filaments of the cytoskeleton with higher contrast than in

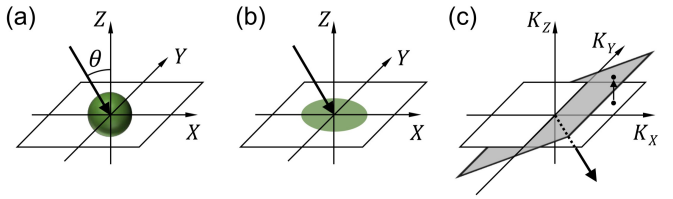

Fig. 2. Projection operation performed by an off-axis tube lens and the inverse projection operation to reconstruct the 3D tomogram. (a) shows the imaging geometry, and (b) shows the projection image recorded with the tube lens translated by X_0, which corresponds to the viewing angle of ϑ. The arrows in (a) through (c) represent the viewing direction of the off-axis tube lens. (c) illustrates the process to map the Fourier transform of the projection image in the 3D spatial frequency space.

Fig. 3(d). Comparing the contrast ratio of the two actin filaments shown in Figs. 3(c) and 3(f), sliding tomography provides about 0.22 and 0.31, while the objective focus scan provides about 0.05 and 0.12, respectively. Here the contrast ratio was defined as $(I_{max} - I_{min})/(I_{max} + I_{min})$, where I_{max} and I_{min} are the maximum and minimum intensity values in the profile. Figure 3(b) shows a cross section of the reconstructed tomogram at a different height where mitochondria are conspicuously seen. As with the actin filaments, the mitochondria can be seen more clearly in Figs. 3(b) than in Fig. 3(e). For fair comparison, regularization or deconvolution has been excluded; thus, the difference between the two dataset can be attributed to the data collection methods or the sampling strategies. As will be shown later, the transverse resolution of sliding tomography is almost the same as that of the objective-focus scan method. The high visibility of the organelles seen in Figs. 3(a) and 3(b) is attributed to the high axial resolution of sliding tomography in comparison with the objective-focus scan for the same numerical aperture.

We measured the 3D PSF of sliding tomography using a 0.1 µm fluorescent bead. The reconstructed tomogram was averaged along the polar coordinate in each horizontal cross section. The horizontal (X-Y) and vertical (Y-Z) cross sections of the 3D PSF for sliding tomography are shown in Figs. 4(a) and 4(b), respectively. The transverse and axial profiles of the 3D PSF are shown in Figs. 4(c). The full-width at half maximum (FWHM) is 0.72 µm along the transverse direction and 2.96 µm along the axial direction, which may be used as an estimate for the resolution. For comparison, the 3D PSF of the objective-focus scan method was obtained by recording a stack of 200 images for the same 0.1 µm bead with the step size of 50 nm. Correcting for the refractive index mismatch[10], the step size in the sample volume was 43.7 nm. The recorded 3D PSF was averaged along the polar coordinate in each horizontal cross section. The horizontal (X-Y) and vertical (Y-Z) cross sections of the resulting 3D PSF are shown in Figs. 4(d) and 4(e), respectively. The transverse and axial profiles of the 3D PSF for the objective-focus scan method are shown in Figs. 4(f). The FWHM is 0.74 µm for the transverse profile and 3.84 µm for the axial profile.

Fluorescence microscopy is a workhorse technology in biology research. A variety of techniques have been developed to increase the spatial resolution[11], the data acquisition speed[8, 12–16], and the number of probes that can be simultaneously imaged[17, 18]. For 3D fluorescence imaging, the objective-focus scan in combination with deconvolution is the most accessible, and thus most popular method. Here we have demonstrated a 3D fluorescence microscopy technique which replaces the axial scan of the objective lens with the lateral scan of the tube lens. The so-called sliding tomography directly records the projection images corresponding to varying viewing directions without rotating the sample. Using the Fourier slice theorem, the 3D distribution of fluorophores in the imaged specimen can be reconstructed from the recorded projection images. Imaging BPAE cells and 0.1 µm beads, we have shown that sliding tomography provides horizontal cross-sections with higher visibility and less hazy background than the objective-focus scan owing to the 23% higher axial resolution for the same numerical aperture. Using wide-field imaging, sliding tomography minimally exposes the sample to the excitation light, and thus provides a minimally phototoxic 3D imaging method[19]. The translation stage used for the tube lens scan does not require high accuracy, while a piezo stage with nanometer precision is necessary for the objective-focus scan. The cost is the reduction of the field of view to about 1/2 along the direction of the tube lens translation.

ACKNOWLEDGEMENT

This research was funded by the National Science Foundation (1808331) and the National Institute of General Medical Sciences of the National Institutes of Health (R21GM135848).

DISCLOSURE

The author declares no conflicts of interest.

REFERENCES

1. J. Sharpe, U. Ahlgren, P. Perry, B. Hill, A. Ross, J. Hecksher-Sørensen, R. Baldock, and D. Davidson, Science **296**, 541 (2002).
2. A. C. Kak and M. Slaney, Principles of computerized tomographic imaging (IEEE press New York, 1988).
3. J. Sharpe, Annu. Rev. Biomed. Eng. **6**, 209 (2004).
4. J. R. Walls, J. G. Sled, J. Sharpe, and R. M. Henkelman, Phys. Med. & Biol. **52**, 2775 (2007).
5. M. R. Arnison, C. J. Cogswell, C. J. Sheppard, and P. Török, "Wavefront coding fluorescence microscopy using high aperture lenses," in Optical Imaging and Microscopy: Techniques and Advanced Systems, (Springer, Heidelberg, 2003), pp. 143–165.
6. Q. Miao, J. R. Rahn, A. Tourovskaia, M. G. Meyer, T. Neumann, A. C. Nelson, and E. J. Seibel, J. Biomed. Opt. **14**, 064035 (2009).
7. T. Kolb, S. Albert, M. Haug, and G. Whyte, J. Biophotonics **8**, 239 (2015).
8. Y. Sung, Phys. Rev. Appl. **13**, 054048 (2020).
9. Y. Sung, Phys. Rev. Appl. **15**, 064065 (2021). Publisher: APS.
10. T. D. Visser, J. L. Oud, and G. J. Brakenhoff, Optik **90**, 17 (1992).
11. L. Schermelleh, A. Ferrand, T. Huser, C. Eggeling, M. Sauer, O. Biehlmaier, and G. P. Drummen, Nat. Cell Biol. **21**, 72 (2019).
12. M. Levoy, R. Ng, A. Adams, M. Footer, and M. Horowitz, ACM Trans. Graph. **25**, 924 (2006).
13. A. Llavador, J. Sola-Pikabea, G. Saavedra, B. Javidi, and M. Martínez-Corral, Opt. Express **24**, 20792 (2016).
14. L. Cong, Z. Wang, Y. Chai, W. Hang, C. Shang, W. Yang, L. Bai, J. Du, K. Wang, and Q. Wen, eLife **6** (2017).
15. G. Scrofani, J. Sola-Pikabea, A. Llavador, E. Sanchez-Ortiga, J. C. Barreiro, G. Saavedra, J. Garcia-Sucerquia, and M. Martínez-Corral, Biomed. Opt. Express **9**, 335 (2018).
16. C. Guo, W. Liu, X. Hua, H. Li, and S. Jia, Opt. Express **27**, 25573 (2019).
17. A. M. Valm, R. Oldenbourg, and G. G. Borisy, PLoS One **11**, e0158495 (2016). Publisher: Public Library of Science San Francisco, CA USA.
18. C. Juntunen, I. M. Woller, and Y. Sung, Sensors **21**, 3652 (2021).
19. P. P. Laissue, R. A. Alghamdi, P. Tomancak, E. G. Reynaud, and H. Shroff, Nat. Methods **14**, 657 (2017).

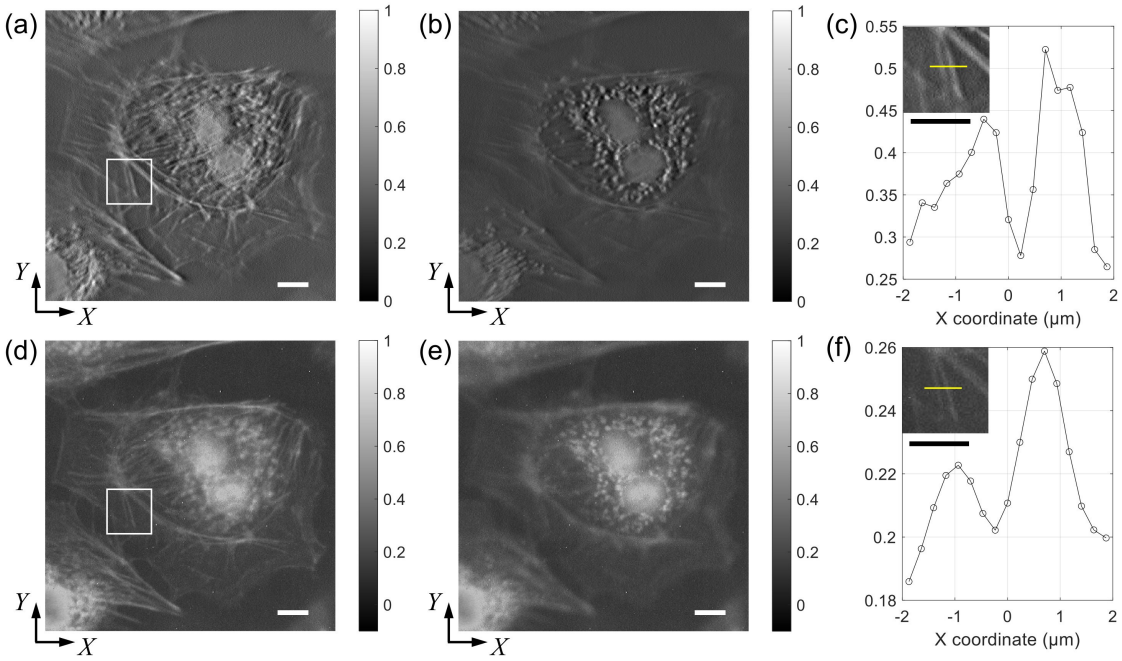

Fig. 3. An example of the reconstructed tomogram and its comparison with the axial stack acquired with the objective focus scan method. (a) and (b) are horizontal (i.e., X-Y) cross sections of the reconstructed tomogram, which are axially separated by 3.3 μm. The square region in (a) is magnified and shown in (c), together with the profile along the line. (d) and (e) are the wide-field images at the heights corresponding to (a) and (b), respectively. The square region in (d) is magnified and shown in (f), together with the profile along the line. Scale bars in (a) through (f): 10 μm.

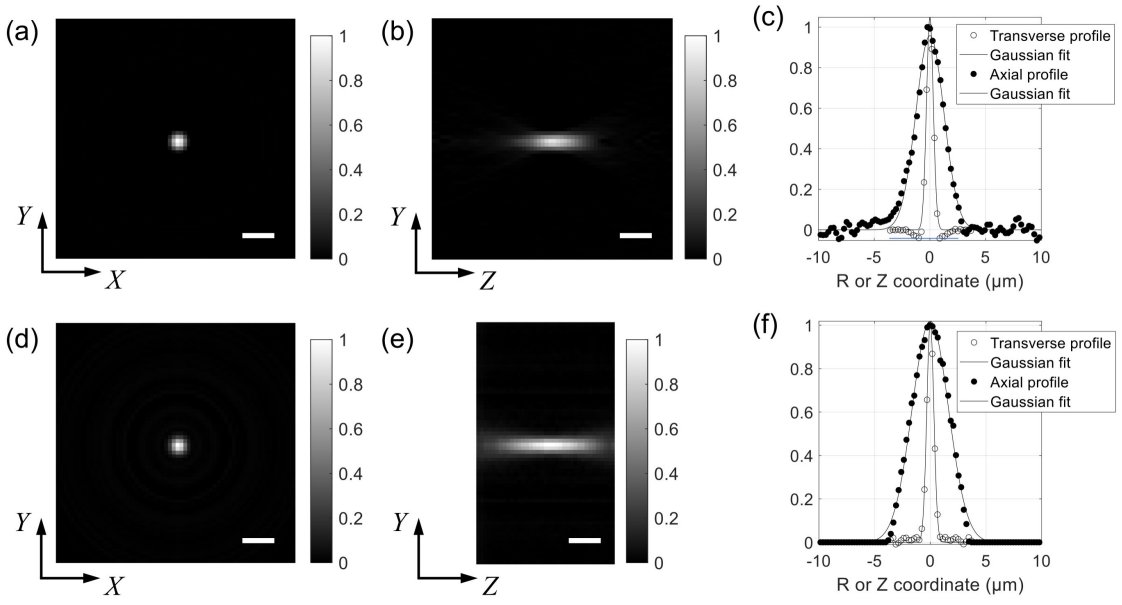

Fig. 4. Three-dimensional point spread functions (PSFs) of sliding tomography and the objective-focus scan method, which were acquired with a 0.1 μm-diameter bead. (a) and (b) are the horizontal (i.e., X-Y) and vertical (i.e., Y-Z) cross sections, respectively, of the 3D PSF. (c) is the intensity profile along the radial (R) or the Z coordinate. (d) and (e) are the horizontal and vertical cross sections, respectively, of the 3D PSF for the axial stack of images acquired with the objective-focus scan. (f) is the intensity profile along the radial (R) or the Z coordinate. The 3D PSFs measured with the bead were averaged along the polar coordinate in each horizontal cross section. The transverse and axial resolutions determined with the full-width at half maximum (FWHM) are 0.72 μm and 2.96 μm for the proposed method, and 0.74 μm and 3.84 μm for the objective-focus scan. Scale bar: 2 μm.